Wrinkling measurement of the mechanical properties of drying salt thin films

*Giulia L. Ferretti‡, Manuela Nania‡, Omar K. Matar, João T. Cabral**

Department of Chemical Engineering, Imperial College London, London SW7 2AZ, UK

We report a time-resolved approach to probe the mechanical properties of thin films during drying and solidification based on surface wrinkling. The approach is demonstrated by measuring the modulus of a ternary system comprising an inorganic salt (aluminium chlorohydrate), a humectant (glycerol) and water across the glassy film formation pathway. The topography of mechanically-induced wrinkling of supported films on polydimethylsiloxane (PDMS) is experimentally monitored during mechanical extension and relaxation cycles. Non-trivial aspects of our method include the need to oxidise the (hydrophobic) PDMS surface prior to solution deposition to enable surface wetting, which simultaneously creates a glassy-layer skin, whose wrinkling can contribute to the overall topography. Film drying is studied as a function of solution concentration and time, and a range of pattern morphologies are found: sinusoidal wrinkling, transient double-wavelength wrinkling accompanying film 'crust' formation, ridging associated with stress localization, and cracking. We quantify the evolution of the elastic modulus during the sinusoidal wrinkling stage, employing bi- and tri-layer models, which are independently confirmed by nano-indentation. The method provides thus a simple and robust approach for the mechanical characterization of out-of-equilibrium thin films.

1. Introduction

Measuring the evolution of mechanical properties of thin films is of fundamental importance for applications ranging from paints, foods, agrochemicals and personal care, including deodorants and cosmetics[1]. Time-resolved measurements of composition, microstructure[1] and elastic modulus[2] are important not only to understand evaporation and film formation pathways, but also the role of environmental fluctuations, e.g., humidity and temperature.

Spontaneous surface wrinkling of laminate films can occur as a result of mechanical stress[3, 4, 5, 6], expansion and contraction associated thermal deposition, or during solvent evaporation and shrinkage [7, 8, 9, 10, 11], and is often undesirable[7, 8, 11, 12, 13, 14, 15]. The analysis of wrinkling topographies has also been shown to provide a powerful tool for the mechanical characterisation of thin and ultra-thin polymeric, composite and metallic supported thin films[2, 7, 16, 17, 18].

In this study, we build upon the well-known SIEBIMM[18, 19] wrinkling method and adapt it for the time-resolved measurement of the mechanical properties of thin films upon drying in a controlled environment. We seek to overcome the difficulties associated with handling very thin free-standing films and the limited sensitivity of conventional methods[2], and resolve aspects of directional solidification, including crust formation[20]. As a model system for our study, we select a ternary blend comprising an inorganic salt, aluminium chlorohydrate (ACH), and a humectant, glycerol, in water. These components constitute the base formulation of antiperspirants, one of the largest health and beauty product categories, whose rheo-mechanical behaviour and speciation remains poorly understood[21,22]. In part, this is due to ACH behavior as an 'inorganic polymer' in aqueous solution.[22] Dialuminium chloride pentahydroxide (DACPH), used in this study, is the most common form of ACH for such thin film application. This system forms a glass upon water loss and film formation, and

crystallisation is not observed unlike other ACH species.[21, 22, 23, 24] Glass formation was confirmed for all conditions investigated in this study (supporting information Figures SI1 and SI2). We expect diverse buckling responses as a function of composition and environmental conditions due to its distinctive non-monotonic behaviour, for instance, of drying kinetics and final composition on glycerol content and relative humidity[25]. Previous studies on skin ageing and wrinkling, reviewed by Genzer and Groenewold,[16] and qualitative analysis of drying gelatin films[1] have also reported a range of pattern morphologies.

The implementation of our approach requires the simultaneous wetting of the substrate by the ternary solution, to enable planar film formation, and simultaneous impermeability of the support, preventing inadvertent composition and dimensional changes. Further, directional drying of liquid films can be expected to result in film stratification and 'crust' formation[20] and, in turn, departure from single frequency sinusoidal wrinkling towards more complex modes, including wrinkling cascades[16, 26], folding and ridging[26, 27]. Different wrinkling models must therefore be tested and validated in order to extract information about film mechanical properties throughout the drying pathway.

Our paper is structured as follows: Section 1.1 reviews the fundamental wrinkling equations and experimental plan while Section 1.2 describes the model system. Section 2 details the solution preparation and optimisation of substrate modification, and the experimental methods employed to characterise the wrinkling patterns. In Section 3, we map the wrinkling morphologies obtained as a function of film composition and drying time, and compute the evolution of the film modulus with time within the sinusoidal wrinkling regime. The results are validated by nanoindentation and discussed in terms of the ternary solution behaviour. A summary of our findings and conclusions is presented in Section 4.

1.1 Mechanical wrinkling of bi- and trilayer films

Sinusoidal wrinkling occurs by mechanical compression of laminate films with an appropriate mismatch between the moduli of the substrate and the supported layers. Analysis of the surface topography should, in principle, enable the mechanical properties of drying films to be probed, as illustrated by our experimental plan in Figure 1.

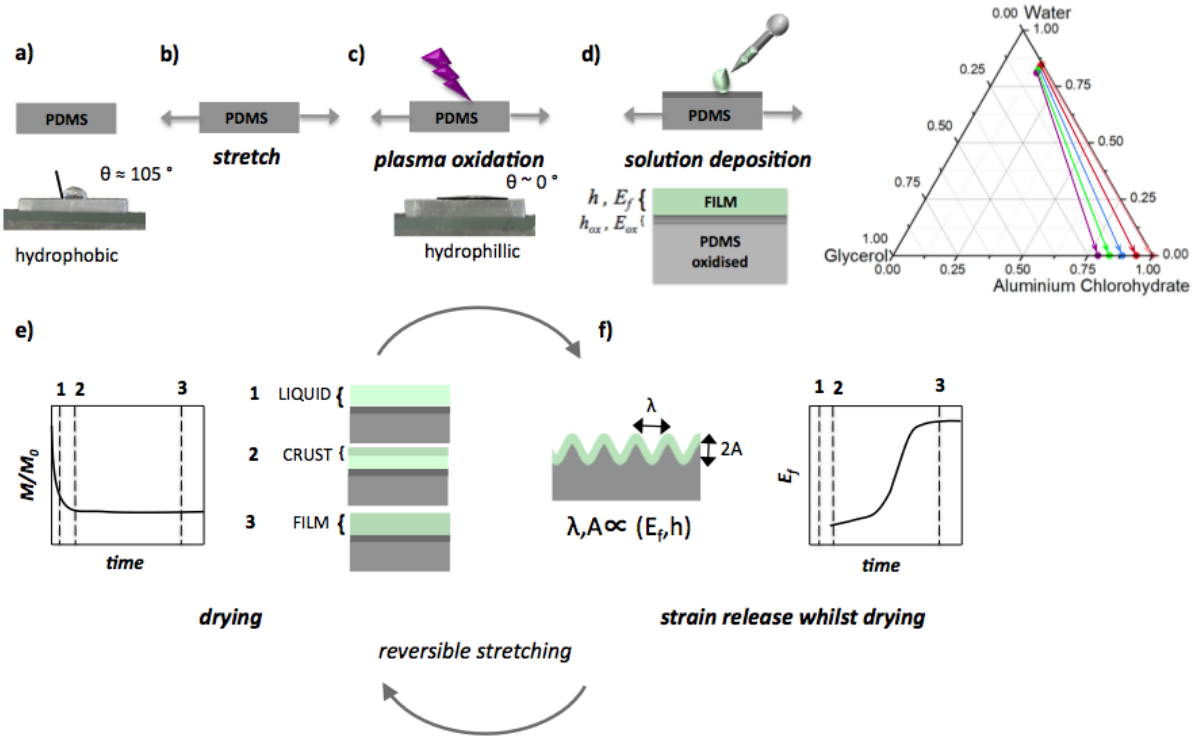

Figure 1: Schematic of the proposed experimental approach. (a) A hydrophobic PDMS substrate is (b) stretched and then (c) oxidised to enable film formation; (d) the solution of interest is then deposited and allowed to dry for prescribed time intervals; the ternary diagram drying pathways as a function of initial solution concentration is illustrated. (e) The liquid film starts drying and may form a transient 'crust' before entirely hardening. During the drying process, the film mass decreases until an asymptote is reached while, (f) the sandwich layer is mechanically interrogated by releasing strain. Topographic analysis of the wrinkling profile enables the calculation of the film's elastic modulus throughout the pathway.

Ternary solutions of prescribed composition are cast onto a thick, pre-stretched, elastomeric polydimethylsiloxane, PMDS, substrates. In order to enable the wetting of the aqueous solution and planar film formation upon drying, PDMS is rendered hydrophilic by surface oxidation, prior to deposition of the solution. Oxidation, however, leads to the formation of a

glassy skin layer,[6] with thickness h_{ox}, supporting the drying aqueous film, of thickness h. Upon strain removal at different stages of drying, various surface patterns emerge, with sinusoidal profiles appearing within an appropriate range of initial solution concentrations and drying times. A simple bilayer model analysis provides a straightforward measurement of film elastic modulus E_i and thickness h_i, from a measurement of sinusoidal wrinkling wavelength λ, and amplitude A, according to [28, 29, 30]

$$\lambda = 2\pi h_i \left(\frac{\bar{E}_f}{3\bar{E}_{PDMS}} \right)^{1/3} \quad (1a)$$

$$A = h_i \left(\frac{\varepsilon}{\varepsilon_c} - 1 \right)^{1/2} \quad (1b)$$

where ε_c is the critical strain

$$\varepsilon_c = \frac{1}{4} \left(\frac{3\bar{E}_{PDMS}}{\bar{E}_f} \right)^{2/3} \quad (1c)$$

and ε is prestrain ($\varepsilon > \varepsilon_c$), defined as the ratio between the sample's length after stretching and the initial length, $\bar{E}$ the plane strain modulus, related to the Young's modulus through $\bar{E} = E/(1-\nu^2)$, and ν is the respective Poisson ratio. In this study, we assume a Poisson's ratio of 0.5 for PDMS[31] and 0.27 for the inorganic salt film[32]. The presence of a significant glassy SiO_x skin layer of the PDMS surface, caused by the oxidation treatment, may however require a third, explicit layer, between the PDMS and the drying aqueous film, shown in dark grey in Figure 1d. We refer to the tri-layer model proposed by Nolte et al.[33] which extends eqs. 1a,b and c by replacing the elastic modulus of the film by an effective modulus ($\bar{E}_{eff}$), depending on the moduli of the top film $\bar{E}_f$ and glassy PDMS oxide layer $\bar{E}_{ox}$. $\bar{E}_{eff}$ is then directly computed from a wrinkling experiment (eqs. 1a,b), while $\bar{E}_{ox}$ is independently determined[4, 6] in the absence of a top film. The property of interest, $\bar{E}_f$, can thus be obtained, according to:

$$\overline{E_f} = \frac{\overline{E_{eff}} - \overline{E_{ox}} \cdot \left[\left(\phi_{ox} - \frac{k}{2} \right)^3 + \left(\frac{k}{2} \right)^3 \right]}{\left[\left(1 - \frac{k}{2} \right)^3 - \left(\phi_{ox} - \frac{k}{2} \right)^3 \right]} \qquad (2)$$

where

$$k = \frac{1 + \phi_{ox}^2 \left(\frac{\overline{E}_{ox}}{\overline{E}_f} - 1 \right)}{1 + \phi_{ox} \left(\frac{\overline{E}_{ox}}{\overline{E}_f} - 1 \right)}, \quad \text{and} \qquad \phi_{ox} = \frac{h_{ox}}{h + h_{ox}} \qquad (3)$$

One can expect that, if h_{ox} is sufficiently small, the difference between eqs. (1a,b) equations (1) and the value obtained through equations (2-3) becomes negligible and $\overline{E}_{eff} \approx \overline{E}_f$. The applicability of both models is assessed below.

1.2 Ternary salt/glycerol/water model system

Hydroxyaluminium solutions have diverse applications such as coagulants in waste water treatments, catalyst support in pillared clays[34] as well as being the main active ingredient in antiperspirant formulations[23, 24]. The system studied is a ternary mixture, composed of aluminium chlorohydrate (ACH) – specifically dialuminium chloride pentahydroxide – and glycerol in water. Both components are highly hygroscopic in nature and the competitive binding between all three components results in non-monotonic drying kinetics and dry film composition. At conditions of 25°C and 25% RH, only water is lost during film formation. The system forms a glass upon drying, by contrast with other ACH species.[21,22] Glass formation was confirmed experimentally via X-ray diffraction and calorimetry, when ACH concentrations reach or exceed 63wt% and for glycerol concentrations below 37wt%[25]; crystallisation is not observed across the composition range and drying pathways investigated (Supporting Information Figures SI1 and SI2).[21, 22, 23, 24] Viscosity measurements and tack

tests established a tack transition boundary extending beyond the glassy region, and that a transient (non-tacky) skin can form during evaporation of sufficiently thick films[25]. We thus seek to resolve the evolution of the mechanical properties of this complex ternary solution along its drying pathway via mechanical wrinkling.

2. Experimental

2.1 Polydimethylsiloxane substrate preparation and oxidation

Polydimethylsiloxane (PDMS) sheets of 5 mm thickness were prepared from Dow Sylgard Kit 184. The elastomer and the cross-linker, in a mass ratio of 10:1, were mixed, cast on a glass plate and allowed to cure for 3 hours at ambient temperature and 1 hour at 75°C. The slabs were then cut into 3 cm x 1.5 cm rectangles, with modulus measured to be E_{PDMS}=1.6 MPa. PDMS is a convenient substrate for wrinkling experiments, due to its near-incompressibility (Poisson ratio $\nu \approx 0.5$[31]), tuneable modulus and large elongation at break ($\varepsilon \approx$ 200%[35]). However, while PDMS substrates readily form laminates with floated or evaporated films[8, 17, 36, 37], with good interfacial bonding, solution deposition requires surface wetting and thus modification of the otherwise hydrophobic elastomer. We oxidise the PDMS coupons by plasma air plasma exposure or UV ozonolysis[3, 4, 6]. To minimise crack formation, surface oxidation takes place under strain, employing a uniaxial strain stage and stretching the coupon by $\varepsilon \approx 20\%$. Air plasma oxidation is carried out using a Harrick Plasma PDC-002, with air pressure P = 1 mbar, power p = 7 W, and exposure times t = 2, 20 and 40 min. Plasma exposure causes the surface CH_3 groups to be converted into OH groups[38, 39, 40, 41], resulting in the formation of a glassy-like layer of defined thickness, which becomes thicker as the oxidation time increases[4, 6]. The oxidised PDMS is thus hydrophilic, permitting full wetting of the aqueous solution and planar film formation. UVO oxidation is carried out within a UV-Ozone cleaner (PSD Pro Series NOVASCAN) with exposure times t= 60, 90 and 120 min,

where the sample is placed at a distance of ~1cm from the lamp.

2.2 Model solution preparation and film drying

Ternary solutions of aluminium chlorohydrate (50wt% hydrated dialuminium chloride pentahydroxide aqueous solution, Summit Research Labs Inc.), glycerol (purity ≥99.5%, Sigma-Aldrich) and deionised water (obtained from a MilliQ source) were prepared, homogenised and equilibrated overnight. The solutions were formulated with fixed initial ACH composition of 15wt% and varying initial glycerol mass compositions ranging from 0wt% to 15wt%, with the remainder of the solution being composed of water. As water is solely lost from the system upon drying[25] and the initial mass fraction of ACH is constant in all solutions, the compositions are indicated via the mass fraction of glycerol in the original solution, $c_{0,glycerol}$, throughout the paper.

An initial wet film thickness of ≈30 μm was deposited on pre-stretched, oxidised PDMS coupons, by covering an area of 1.5 cm x 1.5 cm with a volume of 7 μL of solution. The liquid films were allowed to dry over time, at ambient temperature (25°C) and relative humidity of 25%, while mass changes were monitored with a Sartorius 1702 balance.

Throughout drying, pre-strain was periodically relaxed to interrogate the surface wrinkling pattern. We refer to these as 'ON' samples, as wrinkling appears in the relaxed state, as opposed to 'OFF' samples, where patterns become visible upon straining. The latter are found to be more likely to form cracks (see Supporting Information Figure SI3), in addition to requiring surface profiling under stress.

2.3 Surface pattern visualization and analysis

Upon strain removal, wrinkling patterns were analysed by optical microscopy (Olympus BX

41M), in order to qualitatively establish the relationship between pattern formation and solution composition. Quantitative surface profile measurements were obtained by stylus profilometry, using a Bruker DektakXT DXT equipped with a 12.5 μm radius stylus. Selected samples were further analysed by atomic force microscopy (AFM) using a Bruker Innova microscope in tapping mode at 0.2 Hz with Si tips (MPP-11100 W, Bruker).

3. Results and discussion

3.1 Substrate oxidation for minimal impact in drying kinetics

PDMS surface oxidation is required to ensure wetting of the drying aqueous solutions. Control experiments were thus carried out to assess the possible impact of the process on film drying kinetics. An impermeable polyester support sheet is used as a reference substrate. The overall mass of PDMS support and film is measured, and then mass evolution *M(t)* of the ternary solution film estimated. Normalised mass loss curves *M(t)/M(t=0)* where t is drying time, for different plasma exposure doses are shown in Figure 2, for identical drying conditions (T=25°C and RH=25%).

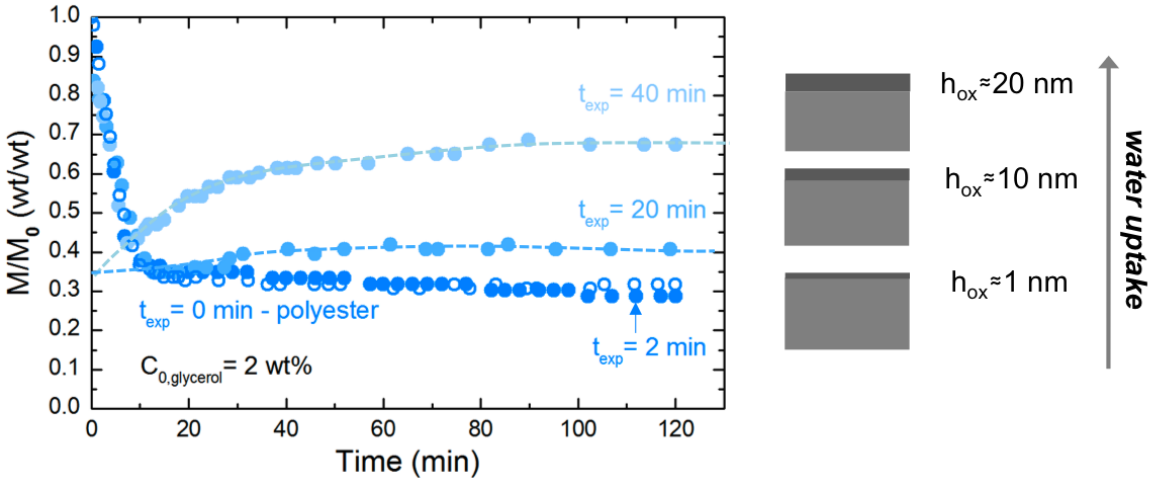

Figure 2: Normalised mass loss of a film of initial glycerol composition $c_{0,glycerol}$=2 wt% during drying (T=25°C and RH=25%) on various substrates: (○) a polyester sheet (impermeable reference) and (●) PDMS oxidised in air plasma at P=1

mbar and p=7 W, for 2-40min. Increasing oxidation causes PDMS swelling by water uptake, but a t_{exp}=2 min plasma exposure yields wetting surfaces with comparable drying profile to the polyester reference.

We find that, for the longer plasma exposures (t_{exp} = 20 and 40 min), after an initial mass loss decay due to water evaporation, the film mass *appears* to increase again at long times. Evidently, long plasma exposures cause the hydrophilic PDMS to uptake water and swell, at timescales commensurate with film drying. However, shorter plasma exposures cause negligible swelling, yielding mass loss profiles indistinguishable from the control measurements, and enabling surface wetting and planar film formation. A plasma exposure t_{exp}=2 min was found to be optimal and employed for the remainder of the study.

3.2 Wrinkling morphologies as a function of dry film composition

Films with different initial compositions were allowed to dry for selected time intervals on 2 min oxidised, pre-stretched by $\varepsilon \approx 20\%$, PDMS supports. The contrast between the mechanical properties of the film and the substrate resulted in a variety of patterns observed upon strain removal. At early drying times ($t \leq 10$ min) or for samples with high glycerol (>4%) content, the liquid film surface remained planar, as shown in Fig 3a. Solutions with initial concentration of glycerol ($c_{0,glycerol}$ = 2 wt%) between 0 and 3 wt% exhibited two stages of sinusoidal pattern formation. At drying times between 10 and 12 min, double-frequency sinusoidal profiles are observed, akin to a wrinkling cascade[26, 42], as shown in Fig. 3b. We associate this behaviour with a transient 'crust'[20] formed during rapid evaporation, effectively creating an additional surface skin at intermediate times. Nested wrinkling patterns have been observed in mechanically stretched PDMS treated by UVO oxidation,[42] known to form a gradient structure consisting of a top and intermediate oxide layers and substrate[42, 43], with decreasing elastic moduli. The wavelengths observed during film drying are much larger than those due to the PDMS oxidized skin under the conditions chosen (air plasma, t_{exp}=2 min,

P=1 mbar and p=7.16 W, detailed in supporting information Table SI1 and Figs SI8-9), and shown to be spatially decoupled in in Section 3.3.1. Instead, the directional solidification during drying under these conditions causes the formation of a transient, stiff, skin corroborated by tack measurements[25]. This additional topmost skin forms at the early stages of drying and eventually merges with the 'bulk' layer.

We expect that the short wavelength wrinkles (λ~3μm) arise due to the contrast between the top skin and intermediate layer, while the long wavelength profile (λ~30 μm) arises due to the dominant intermediate layer and the substrate, persisting over longer times. For $20 \leq t \leq$ 120 min (Fig. 3c), only single frequency sinusoidal wrinkles form, readily enabling the mechanical characterisation of the drying film, as discussed above. Eventually, after 120 min, delamination and cracking prevail (Fig. 3d), as the films become excessively brittle upon full water loss.

The effect of PDMS prestretch (ε) on the resulting pattern morphology was evaluated within the sinusoidal range (Supporting Information Fig. SI5): we find a critical value of $\varepsilon_c \approx 15\%$ (for a film of $c_{0,glycerol}$ = 2wt% at 12min drying time), which must be exceeded for wrinkling to be observed. The value of ε_c depends on the ratio between the elastic modulus of the film and the substrate, and a prestrain of ε =20% was thus chosen for the experiments as it exceeds ε_c for this system and range of conditions.

Initial glycerol concentrations of ≈ 4 wt% lead to more complex pattern morphologies, evolving from double scale wrinkling (Fig. 3e) to ridge formation (Fig. 3f-g) with increasing drying time. Sinusoidal wrinkling is expected for $\varepsilon > \varepsilon_c$ and below ε_L, where nonlinearities in the strain energy functions cause stress localisation[26, 27, 44]. The presence of ridges at 4wt% glycerol concentration suggests that $\varepsilon_L \leq 20\%$ and that $\varepsilon_c \approx \varepsilon_L$, since no pattern formation was observed below 20% strain.

Films with 5-15wt% initial glycerol concentration did not exhibit wrinkling at any time during drying, even for prestrains up to 40%. Evidently, either $\varepsilon_c > 40\%$, corresponding to a relatively low modulus contrast ($E_f < 10$ MPa) with respect to the PDMS substrate, or the film remains a viscous liquid throughout, relaxing rapidly any surface pattern form under compression. The addition of glycerol, a well-known plasticiser, above 4 wt% promotes film flexibility and decreases the film's elastic modulus sufficiently to suppress wrinkle formation.

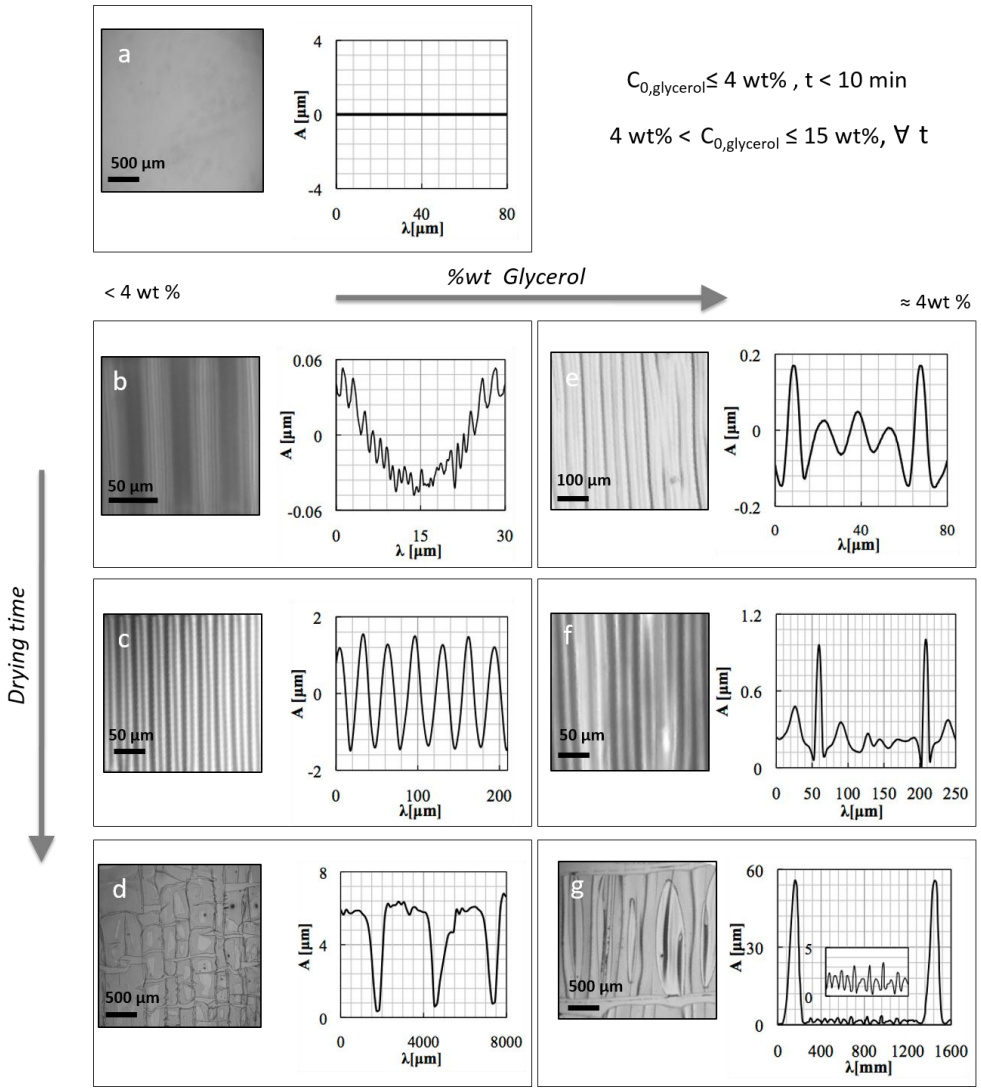

Figure 3: Optical microscopy, profilometry and AFM data of surface patterns observed in the films upon strain removal after drying. a) Absence of wrinkles ($c_{0,glycerol}$= 0-3 wt% , t < 10 min, $c_{0,glycerol}$>4 wt% ,for all drying times). b) Wrinkling cascade ($c_{0,glycerol}$=2 wt% , t=10 min) c) Sinusoidal wrinkles ($c_{0,glycerol}$=2wt% , t=12 min. d) Film fracture and crack formation ($c_{0,glycerol}$=2 wt% , t=150 min) . e-f-g) Patterns deriving from stress localisation and ridging effects ($c_{0,glycerol}$=4wt %, t = 30

min- 2 h). All data refer to drying conditions of T=25°C and RH=25% and PDMS substrates oxidised at P=1 mbar p=7 W and t_{exp}=2 min.

The different wrinkling regimes observed as a function of film composition are mapped onto a ternary diagram in Fig. 4a, including regions where wrinkling does not occur ($\varepsilon<\varepsilon_c$), sinusoidal wrinkles ($\varepsilon_c\leq\varepsilon\leq\varepsilon_L$), and stress localisation and ridging ($\varepsilon\geq\varepsilon_L$), crack-formation and delamination. Within the sinusoidal wrinkling region, we subdivide a range of concentrations (and corresponding drying times at T=25°C at 25% RH) for which double-frequency sinusoidal wrinkling is observed and referred to as a wrinkling cascade.

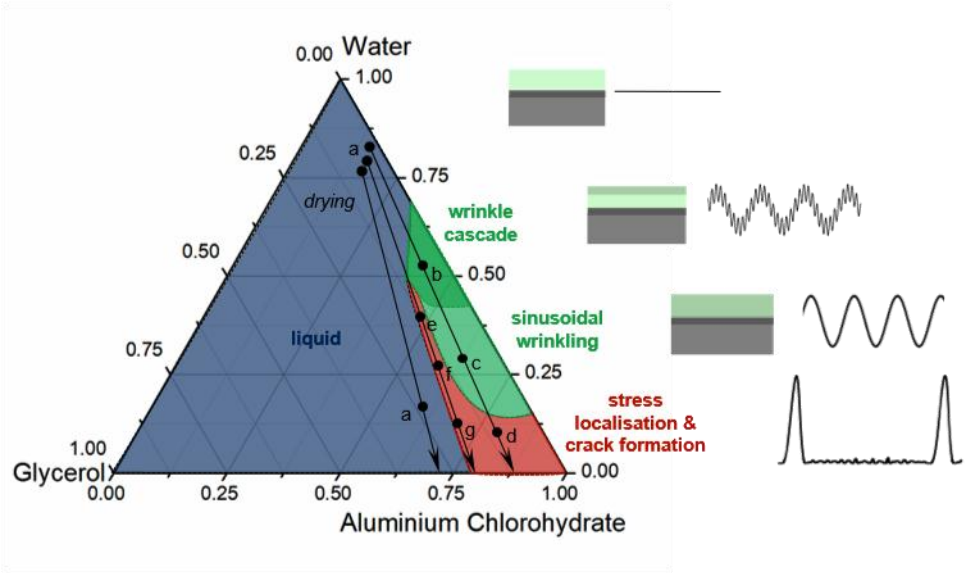

Figure 4: Different pattern formation regimes observed as a function of film composition mapped on the ternary diagram along with the schematic of the corresponding surface profiles. The arrows represent drying pathways for $c_{0,glycerol}$ > 4wt %, $c_{0,glycerol}$ ≈ 4wt % and $c_{0,glycerol}$ < 4wt %, and the letters a-g correspond to the panels in Fig 3.

3.3 Elastic modulus evaluation for sinusoidal wrinkles

3.3.1 Effect of drying time

The evolution of the mechanical modulus of the drying films was analysed within the sinusoidal wrinkling region, by directly measuring λ and A, for which models are well

established. To select the appropriate bi- or tri-layer model, outlined in Section 1.1., the possible effect of the glassy oxide layer formed during PDMS surface treatment needs to be evaluated. For this purpose, neat PDMS, prestretched by 20%, was oxidised using air plasma and UV ozonolysis for various times, and the characteristic wrinkling wavelength λ_{PDMS} and amplitude A_{PDMS} observed upon strain release recorded. Air plasma exposure, carried for time intervals ranging from 90 s to 1 h, resulted in wrinkling with characteristic wavelengths from ≈ 100 nm to ≈ 4 μm, and amplitudes within ≈ 10 nm and ≈ 1 μm (Supporting Information Table SI1, Figure SI 9). At long exposure times, when the oxidised layer reaches saturation, the aspect ratio (A/λ) of the topography becomes constant, as expected from eqs. (1), and detailed in Supporting Information, Figure SI8. UVO exposure, carried for time intervals ranging between 1 and 2 h, resulted in wrinkling with λ ≈ 30 μm to ≈ 80 μm, measured via profilometry (Supporting Information Table SI2), whose aspect ratio, within this range, has not saturated (Supporting Information, Figure SI10). Using eqs. (1a,b), the thickness of the oxide layer h_{ox} was estimated. Then, ternary films with $c_{0,glycerol}$ = 2wt% glycerol were cast onto identical, pre-strained, oxidised layers and the resulting wrinkling profile measured at drying time t=12 min.

Figure 5a plots shows wrinkling wavelength of the drying film, λ_f, as a function of substrate oxidation expressed in terms of the oxidised PDMS wavelength, λ_{PDMS}, ranging from approximately 0.1-100 μm. It is clear that short wavelength PDMS wrinkling has negligible effect of film wrinkling, i.e. $\lambda_{PDMS} << \lambda_f$. However, the effect of substrate wrinkling becomes more important as extent of PDMS oxidation increases, i.e. $\lambda_{PDMS} \approx \lambda_f$, in particular within the UVO range. This observation suggests that a bilayer model might be appropriate when oxidation causes $\lambda_{PDMS} << \lambda_f$, as in short ($t_{exp}$=2 min) plasma exposures, while otherwise a trilayer model should be needed. This hypothesis was proven by calculating the film

Young's modulus considering the existence of the intermediate layer in Fig. 5b. The explicit trilayer results, over the entire range of substrate oxidation, agree with the bilayer model results applied when $\lambda_{PDMS} << \lambda_f$. By contrast, a bilayer assumption in the presence of a thick oxide (intermediate) layer h_{ox} yields inconsistent results for the film modulus under identical drying condition (Supporting Information, Fig. SI11). For the remainder of the data analysis we thus employ a bilayer model, since it provides indistinguishable results for 2 min plasma exposed PDMS substrates.

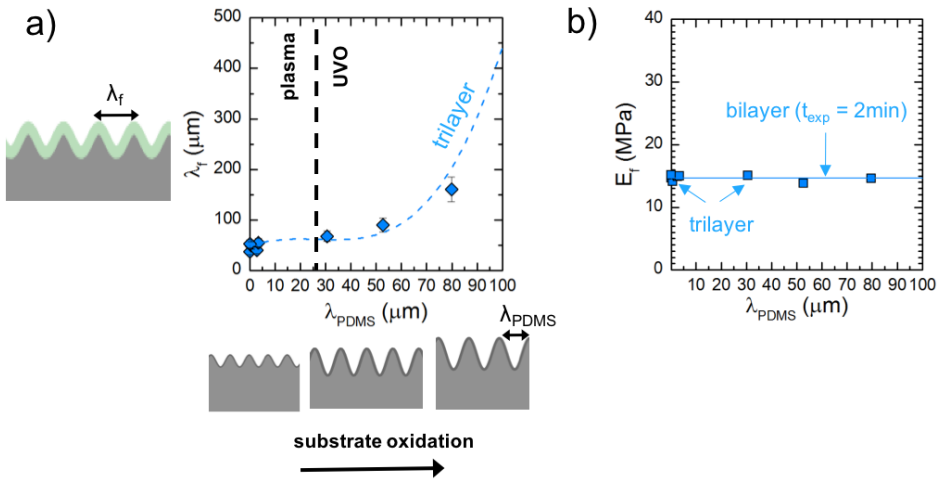

Figure 5: a) Wrinkling wavelength λ_f of $c_{0,glycerol}$ = 2 wt% dried for t=12 minutes as a function of substrate oxidation expressed in terms of the wrinkling wavelength of neat oxidised PDMS under compression λ_{PDMS}. A plasma exposure time t_{exp}=2 min yields λ_{PDMS}= 0.14 μm, while UV exposures reach 10s of μm. When $\lambda_{PDMS} << \lambda_f$, PDMS oxidation does not impact film wrinkling. The dashed line represent the λ_f calculated by using the trilayer model of eqs. (2,3). (b) Elastic modulus of the film evaluated using the trilayer model (■ data) and solid line obtained from the bilayer model with brief PDMS plasma oxidation of t_{exp}=2 min.

Considering the above findings, we next compute the evolution of the Young's modulus of a $c_{0,glycerol}$ = 2wt% film as a function of drying time, shown in Fig. 6f. We first experimentally

measure λ and A of the wrinkling profile observed upon strain removal at different stages of drying, shown in Fig. 6a and b respectively. We then evaluate aspect ratio A/λ, shown in Fig. 6c, which according to eqs. (1a,b) only depends on the film's elastic modulus:

$$\frac{A}{\lambda} = \frac{1}{\pi}\sqrt{\varepsilon - \frac{1}{4}\left(\frac{3\bar{E}_{PDMS}}{\bar{E}_f}\right)^{2/3}} \qquad (4)$$

The evolution of the film's modulus with drying time is shown in Fig. 6f, plotted in a logarithmic scale for comparison with the mass loss, shown in Fig 6d. At short times, the water evaporation ratio is fast, the film remains in the liquid state, and no wrinkling patterns are observed. When the mass loss slows down, after ≈ 12 min for this system, an elastic modulus can be measured and increases rapidly upon further dehydration. This upturn corresponds to a significant increase in viscosity, leading to glass formation and is in good agreement with previous calorimetry experiments[25].

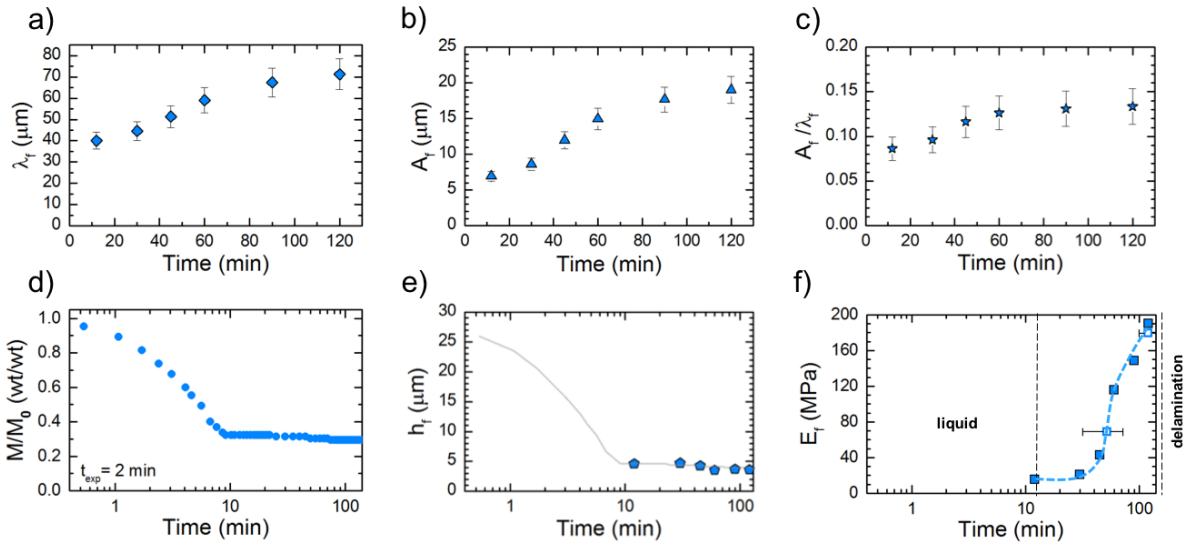

Figure 6: Evolution of drying film properties as a function of time ($c_{0,glycerol}$ = 2wt%, T=25 °C and RH=25%). a) wrinkling wavelength λ_f and b) amplitude A_f observed upon strain release at different drying times and c) corresponding aspect ratio A_f/λ_f. d) Normalised film mass loss as a function of time and e) corresponding height profile from gravimetric data (grey line) and (●) values obtained from wrinkling experiments using the bilayer

model. f) Dynamic evolution of film elastic modulus during drying obtained from (■) wrinkling experiments using the bilayer model, corroborated by (❑) AFM nanoindentation.

As the film stiffens approaching the glass transition (t > 2 h), wrinkling is no longer an effective approach to determine its mechanical properties. Instead, cracking and delamination modes prevail, as seen in Figure 5d, even at low values of prestrain ε = 5-10 %, exceeding ε_c, which itself decreases rapidly at long drying times (Supporting Information Figure SI6). Within this range, AFM nanoindentation can be employed, albeit requiring long measurement times and model-sensitive data analysis (Supporting Information Figure SI7).

From the elastic modulus obtained from our wrinkling approach, it is then possible to estimate the film thickness over time, based on bilayer eqs. (1a,b), as shown in Fig. 6e. The wrinkling values (data points) are found to be in good agreement with the calculated profile from mass loss measurements mass (Fig. 6d), represented as a grey line.

In the measurements reported so far, each data point corresponds to a different sample, which requires the preparation of a large number of specimens. However, the method can be applied continuously on the same film by periodically releasing the stress and then stretching back to the same initial value (Supporting Information Fig. SI4). Some hysteresis in the results can be observed when the same sample is stretched multiple times at low water content, due to progressive delamination and crack formation of brittle samples.

We finally validate the mechanical properties calculated via induced wrinkling by confirming the results with AFM nanoindentation measurements (Fig 6f). While nanoindentation is applicable for such relatively thick films, the measurements are limited by the characteristics of the AFM tips and suffer from substrate convolution for very thin films. By contrast, the wrinkling method is simpler, sufficiently accurate and versatile for these measurements.

3.3.2 Dependence of film modulus on solution concentration

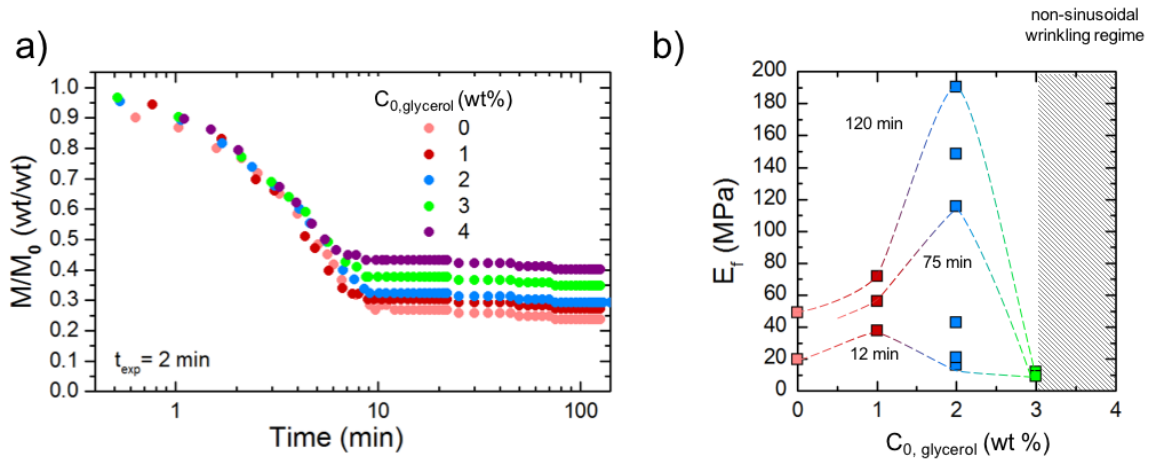

Figure 7: a) Normalised film mass loss for different initial solution compositions (0 wt% < $c_{0,glycerol}$ < 4 wt% and $c_{0,ACH}$ = 15 wt%) upon drying at 25°C and 25% RH. b) Film elastic modulus calculated using a bilayer model as a function of initial solution composition in terms of glycerol content.

We next compute the evolution of the elastic modulus for films of varying initial glycerol compositions ($c_{0,glycerol}$) during drying. Figure 7a shows the recorded normalised mass loss profile over time for films with different initial glycerol compositions. Since glycerol is an effective humectant, increasing its content in the solution increases the final film mass, as more water is retained[25]. Figure 7b shows the elastic modulus of films dried for 12, 75 and 120 min as a function of $c_{0,glycerol}$. As can be seen on the graph, the trend is found to be markedly non-monotonic with glycerol concentration. One might have expected the elastic modulus to decrease with the addition of glycerol as observed previously for $c_{0,glycerol}$ between 5wt% and 15 wt%; however, small glycerol quantities ($c_{0,glycerol} \leq 4$ wt% for $c_{0,ACH}$ = 15 wt%) have been reported to act as an anti-plasticiser,[25,45, 46, 47, 48] and actually increase the film modulus, before the latter eventually decreases as the film becomes liquid at high humectant concentrations (for $c_{0,glycerol}$ > 4%). The competitive binding between glycerol, water and

ACH was shown to result in the replacement of water molecules bound to the salt's hydroxyl groups by glycerol, which enhances film drying. Generally, as the film loses more water its elastic modulus increases as can be observed in the 120min curve in Figure 8 which is above the 12min curve. The 120min elastic modulus trend as a function of composition presented in Figure 8 is in accordance with previous calorimetric measurements[25]. The latter showed vitrification upon water loss solely for $c_{0,glycerol}$ between 0 wt% and 4 wt% with $c_{0,ACH}$ = 15 wt%. Hence wrinkling occurs in glassy samples only in this study, as we have shown previously that glycerol rich films ($c_{0,glycerol} \geq 5$ wt%) remain smooth upon strain release.

4. Conclusion

We have investigated the feasibility of determining the evolution of mechanical properties of thin *drying* films by surface wrinkling analysis. A model system consisting of aluminium chlorohydrate, glycerol and deionised water was allowed to dry on pre-stretched, oxidised PDMS. Substrate oxidation is required for wetting and film formation but, when prolonged, has two adverse effects: (i) increases the PDMS water uptake and (ii) creates an additional layer whose own wrinkling is commensurate with that of the drying film of interest. An optimal short air plasma exposure (2 min, P = 1 mbar, p = 7 W) is found to circumvent both issues. A range of surface patterns emerge during film drying, as a function of composition and time, under uniaxial strain: planar, sinusoidal (both single and double-frequency), ridging and eventual cracking and delamination. The sinusoidal region could be successfully analysed with bi- and trilayer wrinkling models, which are cross-validated and also against nanoindentation measurements. A bilayer wrinkling model, considering only the film and the PDMS substrate, suffices to accurately describe film drying, provided that the PDMS oxide layer is sufficiently thin (and thus $\lambda_{PDMS} << \lambda_{film}$). The method was then employed to study the effect of glycerol (a humectant) addition on the drying of ACH/water films, revealing a

sigmoidal modulus transition with time approaching glass formation and a non-monotonic dependence of modulus on glycerol content, in good agreement with previous work. This time-resolved wrinkling interrogation during film formation emerges thus as a simple and reliable approach to determining evolving mechanical properties of films, with potential applications extending to coatings, personal care and foods.

Supporting Information. A brief statement in non-sentence format listing the contents of material supplied as Supporting Information should be included, ending with "This material is available free of charge via the Internet at http://pubs.acs.org." For instructions on what should be included in the Supporting Information, as well as how to prepare this material for publication, refer to the journal's Instructions for Authors.

AUTHOR INFORMATION

Corresponding Author

*j.cabral@imperial.ac.uk

Author Contributions

GF and MN carried out all experimental work and analysis, assisted by JTC. The manuscript was written through contributions of all authors and all authors have given approval to the final version of the manuscript. ‡These authors contributed equally.

ACKNOWLEDGMENT

We acknowledge the Department of Chemical Engineering, Imperial College London, for PhD studentships for GF and MN, and Andrew Hopkinson (Unilever) for useful discussions.

REFERENCES

(1) Rizzieri, R.; Mahadevan, L.; Vaziri, A.; Donald, A. Superficial Wrinkles in Stretched, Drying Gelatin Films. *Langmuir* **2006,** *22* (8), 3622-3626.

(2) Cranston, E. D.; Eita, M.; Johansson, E.; Netrval, J.; Salajková, M.; Arwin, H.; Wågberg, L. Determination of Young's Modulus for Nanofibrillated Cellulose Multilayer Thin Films Using Buckling Mechanics. *Biomacromolecules* **2011,** *12* (4), 961-969.
(3) Chiche, A.; Stafford, C. M.; Cabral, J. T. Complex micropatterning of periodic structures on elastomeric surfaces. *Soft Matter* **2008,** *4* (12), 2360-2364.
(4) Bayley, F. A.; Liao, J. L.; Stavrinou, P. N.; Chiche, A.; Cabral, J. T. Wavefront kinetics of plasma oxidation of polydimethylsiloxane: limits for sub-mum wrinkling. *Soft Matter* **2014,** *10* (8), 1155-66.
(5) Pretzl, M.; Schweikart, A.; Hanske, C.; Chiche, A.; Zettl, U.; Horn, A.; Böker, A.; Fery, A. A Lithography-Free Pathway for Chemical Microstructuring of Macromolecules from Aqueous Solution Based on Wrinkling. *Langmuir* **2008,** *24* (22), 12748-12753.
(6) Nania, M.; Matar, O. K.; Cabral, J. T. Frontal vitrification of PDMS using air plasma and consequences for surface wrinkling. *Soft Matter* **2015,** *11* (15), 3067-3075.
(7) Qian, W.; Xing, R.; Yu, X.; Quan, X.; Han, Y. Highly oriented tunable wrinkling in polymer bilayer films confined with a soft mold induced by water vapor. *The Journal of Chemical Physics* **2007,** *126* (6), 064901.
(8) Bowden, N.; Brittain, S.; Evans, A. G.; Hutchinson, J. W.; Whitesides, G. M. Spontaneous formation of ordered structures in thin films of metals supported on an elastomeric polymer. *Nature* **1998,** *393* (6681), 146-149.
(9) Breid, D.; Crosby, A. J. Surface wrinkling behavior of finite circular plates. *Soft Matter* **2009,** *5* (2), 425-431.
(10) Guvendiren, M.; Yang, S.; Burdick, J. A. Swelling-Induced Surface Patterns in Hydrogels with Gradient Crosslinking Density. *Advanced Functional Materials* **2009,** *19* (19), 3038-3045.
(11) Chung, J. Y.; Nolte, A. J.; Stafford, C. M. Diffusion-Controlled, Self-Organized Growth of Symmetric Wrinkling Patterns. *Advanced Materials* **2009,** *21* (13), 1358-1362.
(12) Brau, F.; Vandeparre, H.; Sabbah, A.; Poulard, C.; Boudaoud, A.; Damman, P. Multiple-length-scale elastic instability mimics parametric resonance of nonlinear oscillators. *Nat Phys* **2011,** *7* (1), 56-60.
(13) Ohzono, T.; Shimomura, M. Ordering of microwrinkle patterns by compressive strain. *Physical Review B* **2004,** *69* (13), 132202.
(14) Bowden, N.; Huck, W. T. S.; Paul, K. E.; Whitesides, G. M. The controlled formation of ordered, sinusoidal structures by plasma oxidation of an elastomeric polymer. *Applied Physics Letters* **1999,** *75* (17), 2557-2559.
(15) Breid, D.; Crosby, A. J. Effect of stress state on wrinkle morphology. *Soft Matter* **2011,** *7* (9), 4490-4496.
(16) Genzer, J.; Groenewold, J. Soft matter with hard skin: From skin wrinkles to templating and material characterization. *Soft Matter* **2006,** *2* (4), 310-323.
(17) Stafford, C. M.; Harrison, C.; Beers, K. L.; Karim, A.; Amis, E. J.; VanLandingham, M. R.; Kim, H. C.; Volksen, W.; Miller, R. D.; Simonyi, E. E. A buckling-based metrology for measuring the elastic moduli of polymeric thin films. *Nat Mater* **2004,** *3* (8), 545-50.
(18) Stafford, C. M.; Guo, S.; Harrison, C.; Chiang, M. Y. M. Combinatorial and high-throughput measurements of the modulus of thin polymer films. *Review of Scientific Instruments* **2005,** *76* (6), 062207.
(19) Stafford, C. M.; Harrison, C.; Beers, K. L.; Karim, A.; Amis, E. J.; VanLandingham, M. R.; Kim, H.-C.; Volksen, W.; Miller, R. D.; Simonyi, E. E. A buckling-based metrology for measuring the elastic moduli of polymeric thin films. In *Nat Mater*, 2004; Vol. 3, pp 545-550.

(20) de Gennes, P. G. Solvent evaporation of spin cast films: “crust” effects. *Eur. Phys. J. E* **2002,** *7* (1), 31-34.
(21) Laden, K. *Antiperspirants and Deodorants*; Second Edition ed.; Marcel Dekker, Inc.: New York. Basel, 1999; Vol. 20. p 404.
(22) Rowsell, J.; Nazar, L. F. Speciation and Thermal Transformation in Alumina Sols: Structures of the Polyhydroxyoxoaluminum Cluster [Al30O8(OH)56(H2O)26]18+ and Its δ-Keggin Moieté. *Journal of the American Chemical Society* **2000,** *122* (15), 3777-3778.
(23) Pophristic, V.; Klein, M. L.; Holerca, M. N. Modeling Small Aluminum Chlorohydrate Polymers. *The Journal of Physical Chemistry A* **2004,** *108* (1), 113-120.
(24) Teagarden, D. L.; White, J. L.; Hem, S. L. Aluminum chlorohydrate III: Conversion to aluminum hydroxide. *Journal of Pharmaceutical Sciences* **1981,** *70* (7), 808-810.
(25) Ferretti, G. L.; Hopkinson, A.; Cabral, J. T. Phase behaviour and film drying of aluminium chlorohydrate/glycerol/water ternary solutions. *Journal of Colloid and Interface Science* **2015,** *Submitted*.
(26) Chen, Y.-C.; Crosby, A. J. High Aspect Ratio Wrinkles via Substrate Prestretch. *Advanced Materials* **2014,** *26* (32), 5626-5631.
(27) Cao, Y.; Hutchinson, J. W. From wrinkles to creases in elastomers: the instability and imperfection-sensitivity of wrinkling. *Proceedings of the Royal Society of London A: Mathematical, Physical and Engineering Sciences* **2011**.
(28) Allen, H. G. CHAPTER 3 - BUCKLING OF SANDWICH STRUTS. In *Analysis and Design of Structural Sandwich Panels*, Allen, H. G., Ed.; Pergamon, 1969, pp 48-56.
(29) Volynskii, A. L.; Bazhenov, S.; Lebedeva, O. V.; Bakeev, N. F. Mechanical buckling instability of thin coatings deposited on soft polymer substrates. *Journal of Materials Science* **2000,** *35* (3), 547-554.
(30) Huang, R. Kinetic wrinkling of an elastic film on a viscoelastic substrate. *Journal of the Mechanics and Physics of Solids* **2005,** *53* (1), 63-89.
(31) Johnston, I.; McCluskey, D.; Tan, C.; Tracey, M. Mechanical characterization of bulk Sylgard 184 for microfluidics and microengineering. *Journal of Micromechanics and Microengineering* **2014,** *24* (3), 035017.
(32) Nemilov, S. V. Structural aspect of possible interrelation between fragility (length) of glass forming melts and Poisson’s ratio of glasses. *Journal of Non-Crystalline Solids* **2007,** *353* (52–54), 4613-4632.
(33) Nolte, A. J.; Cohen, R. E.; Rubner, M. F. A Two-Plate Buckling Technique for Thin Film Modulus Measurements: Applications to Polyelectrolyte Multilayers. *Macromolecules* **2006,** *39* (14), 4841-4847.
(34) Xu, Y.; Wang, D.; Liu, H.; Yiqiang, L.; Tang, H. Optimization of the separation and purification of Al13. *Colloids and Surfaces A: Physicochemical and Engineering Aspects* **2003,** *231* (1–3), 1-9.
(35) Choi, K. M.; Rogers, J. A. A Photocurable Poly(dimethylsiloxane) Chemistry Designed for Soft Lithographic Molding and Printing in the Nanometer Regime. *Journal of the American Chemical Society* **2003,** *125* (14), 4060-4061.
(36) Chen, Z.; Ren, W.; Gao, L.; Liu, B.; Pei, S.; Cheng, H.-M. Three-dimensional flexible and conductive interconnected graphene networks grown by chemical vapour deposition. *Nat Mater* **2011,** *10* (6), 424-428.
(37) Chae, S. J.; Güneş, F.; Kim, K. K.; Kim, E. S.; Han, G. H.; Kim, S. M.; Shin, H.-J.; Yoon, S.-M.; Choi, J.-Y.; Park, M. H.; Yang, C. W.; Pribat, D.; Lee, Y. H. Synthesis of Large-Area

Graphene Layers on Poly-Nickel Substrate by Chemical Vapor Deposition: Wrinkle Formation. *Advanced Materials* **2009,** *21* (22), 2328-2333.
(38) Owen, M. J.; Smith, P. J. Plasma treatment of polydimethylsiloxane. *Journal of Adhesion Science and Technology* **1994,** *8* (10), 1063-1075.
(39) Demir, M. M.; Menceloglu, Y. Z.; Erman, B. Effect of filler amount on thermoelastic properties of poly(dimethylsiloxane) networks. *Polymer* **2005,** *46* (12), 4127-4134.
(40) Efimenko, K.; Wallace, W. E.; Genzer, J. Surface modification of Sylgard-184 poly(dimethyl siloxane) networks by ultraviolet and ultraviolet/ozone treatment. *J Colloid Interface Sci* **2002,** *254* (2), 306-15.
(41) Hillborg, H.; Gedde, U. W. Hydrophobicity recovery of polydimethylsiloxane after exposure to corona discharges. *Polymer* **1998,** *39* (10), 1991-1998.
(42) Efimenko, K.; Rackaitis, M.; Manias, E.; Vaziri, A.; Mahadevan, L.; Genzer, J. Nested self-similar wrinkling patterns in skins. *Nat Mater* **2005,** *4* (4), 293-297.
(43) Glatz, B. A.; Tebbe, M.; Kaoui, B.; Aichele, R.; Kuttner, C.; Schedl, A. E.; Schmidt, H.-W.; Zimmermann, W.; Fery, A. Hierarchical line-defect patterns in wrinkled surfaces. *Soft Matter* **2015,** *11* (17), 3332-3339.
(44) Cao, Y.; Hutchinson, J. W. Wrinkling Phenomena in Neo-Hookean Film/Substrate Bilayers. *Journal of Applied Mechanics* **2012,** *79* (3), 031019-031019.
(45) Ayadi, F.; Dole, P. Stoichiometric interpretation of thermoplastic starch water sorption and relation to mechanical behavior. *Carbohydrate Polymers* **2011,** *84* (3), 872-880.
(46) Chaudhary, D. S. Competitive plasticization in ternary plasticized starch biopolymer system. *Journal of Applied Polymer Science* **2010,** *118* (1), 486-495.
(47) Chaudhary, D. S.; Adhikari, B. P.; Kasapis, S. Glass-transition behaviour of plasticized starch biopolymer system – A modified Gordon–Taylor approach. *Food Hydrocolloids* **2011,** *25* (1), 114-121.
(48) Godbillot, L.; Dole, P.; Joly, C.; Rogé, B.; Mathlouthi, M. Analysis of water binding in starch plasticized films. *Food Chemistry* **2006,** *96* (3), 380-386.

Table of contents graphic